Acta Metallurgica Sinica (English Letters) (2023) 36:705–716
https://doi.org/10.1007/s40195-023-01528-5

Simultaneously Enhancing Strength, Ductility and Corrosion Resistance of a Martensitic Stainless Steel via Substituting Carbon by Nitrogen

Fuyang Li[1] · Jialong Tian[1] · Huabing Li[1] · L. M. Deineko[2] · Zhouhua Jiang[1]

Received: 12 October 2022 / Revised: 12 December 2022 / Accepted: 22 December 2022 / Published online: 30 January 2023

Abstract
Two martensitic stainless steels of 2Cr12Ni6 type hardened and tempered at 773 K have been studied: the first with 0.2% carbon content and the second with partial replacement of carbon by nitrogen (C0.1N0.1) in the first steel. It is found that the partial substitution of carbon with nitrogen contributed to an increase in ductility and strength of the steel, presumably due to the formation of more dispersive carbonitrides. Meanwhile, the addition of nitrogen suppressed the precipitation of carbonitrides, so that the solid solution strengthening effect of C0.1N0.1 did not decrease significantly after tempering treatment. In addition, the partial replacement of carbon by nitrogen contributed to improved ability against pitting corrosion (PC) in chloride-containing medium (3.5%NaCl at 303 K). The higher resistance to PC of tempered nitrogen-containing steel is apparently due to the lower content of massive carbonitrides, especially the reduced aggregation at grain boundaries. This leads to a lower acidity and aggressiveness of the test solution near the sample surface due to the accumulation of $NH4^+$ ammonium ions in it. As a result of nitrogen addition, exception for $Cr_{23}C_6$ and VC, Cr_2N and (Cr, V) N type precipitates have also been found in C0.1N0.1 steel and this is consistent with the thermodynamic calculation results. In conclusion, substituting carbon by nitrogen in traditional martensitic stainless steel could realize the simultaneous improvement of multiple properties of martensitic stainless steels. This result provides a promising composition optimization route to develop novel martensitic stainless steels.

Keywords Martensitic stainless steel · Strength and ductility · Pitting · Carbonitrides

1 Introduction

Nitrogen is commonly mentioned in the modern metallurgical industry, but has consistently been classified as a hazardous element. In recent years, many studies have found that adding nitrogen into stainless steel could both improve the corrosion resistance and the mechanical properties of steel. In the traditional steel design strategy, the strength was generally enhanced by increasing the carbon content, while this enhancement was invariably accompanied with the loss of plasticity, toughness and the corrosion resistance [1–4]. Moreover, among the various alloying elements added into the steel, nitrogen does not cause environmental problems and nitrogen is also an inexpensive alloying element.

The addition of nitrogen to steel definitely causes an increase in hardness, which has been reported by many researchers [5–7]. However, the effect of nitrogen addition on ductility and toughness is controversial. The effect of nitrogen content on microstructure and mechanical properties of 1Cr12NiMo martensitic stainless steel has been researched. It was found that with the increase in nitrogen content, the strength and hardness of 1Cr12NiMo increase dramatically, while the Charpy impact energy shows a minor decline. This is due to the formation of $M_{23}C_6$, Cr_2N and other carbonitrides toward the grain boundary segregation [8, 9]. Some scholars also carried out experiments on 16Cr5Ni1Mo steel with different nitrogen contents. The results showed that tempering

Available online at http://link.springer.com/journal/40195.

✉ Jialong Tian
neujialong@163.com

✉ Huabing Li
lihb@smm.neu.edu.cn

[1] School of Metallurgy, Northeastern University, Shenyang 110819, China

[2] National Metallurgical Academy of Ukraine, 4, Haharina Ave., Dnipro 49600, Ukraine

above 823 K promotes the precipitation of Cr_2N within martensitic laths and at martensitic lath boundaries, strengthening the alloy at the cost of elongation and toughness [9]. However, in another research [10, 11], the properties of steels with different carbon and nitrogen contents were reported. They showed that adding nitrogen to steel improves its toughness while maintaining its strength. Numerous studies have found that nitrogen alloying has a great effect on the precipitation behavior of carbides in martensitic stainless steel. The addition of nitrogen can significantly reduce the size of carbide and improve the distribution of carbonitrides. At the same time, the precipitation of large phases in martensitic stainless steel was inhibited, and the area proportion of carbides was reduced [12, 13]. It was found that the strength of tempered steel was significantly enhanced, while the impact toughness was not significantly decreased. In this regard, the functional mechanism of nitrogen is not thoroughly understood. The effect of nitrogen on microstructure and mechanical properties of steel still needs to be further studied.

Nitrogen alloying is a common method in modern metallurgy to improve the corrosion resistance of steel. By adding nitrogen to steel, nitrogen can inhibit the nucleation and growth of chromium-rich carbides, which reduces the occurrence of chromium-poor zone at grain boundary. At the same time, with the increase in nitrogen content, the diffusion rate of carbon will slow down. Usually carbon is inclined to form $Cr_{23}C_6$-type carbides, while nitrogen and chromium are inclined to form Cr_2N precipitate. Thus, the content of chromium required for carbon to form carbides is much more than that of nitrogen, so it is difficult to form chromium-poor zone at grain boundaries in nitrogen-containing steel. However, it has been reported that there exists a certain threshold value [14], and the corrosion resistance will decrease if the upper limit of nitrogen content is exceeded.

In this study, the mechanical properties and corrosion resistance of martensitic stainless steel with different contents of carbon and nitrogen were compared. The influence of nitrogen on the strength and plasticity of martensitic stainless steel was systematically discussed. Considering the corrosion resistance, the advantages and disadvantages of introducing nitrogen in martensitic stainless steel with vanadium element have been provided. This study attempts to reveal the functional mechanism of nitrogen through experimental characterization and thermodynamic simulation. The results can deepen the understanding of the role of nitrogen in martensitic stainless steel.

2 Experimental

Two martensitic stainless steels with different carbon/nitrogen additions were melted in a 25 kg vacuum induction melting furnace. Two ingots were homogenized at 1473 K for 8 h and then forged into plates with section size of 25 mm × 80 mm. Steel scrap was taken for analysis. Their compositions in the as-forged state were analyzed by inductively coupled plasma-atomic emission spectroscopy (ICP-AES) and are presented in Table 1.

The sample was solution treated followed by air cooling. Then, the tempering was performed at 773 K for 0.5, 1, 2, 4, 8, 16 and 20 h, respectively, followed by air cooling. In order to obtain the similar grain size in two steels, the solution treatment (The solution temperature is the temperature for dissolving all the precipitates.) has been optimized and will be presented later. The samples for optical microscopy and scanning electron microscopy (SEM) observation were corroded by 2 g picric acid + 5 mL hydrochloric acid + 100 mL ethanol solution [15]. For transmission electron microscopy (TEM) characterization, grind 10 mm × 10 mm × 0.4 mm until the thickness is 40 μm, press the complete wafer with a punch. The electrolysis double spray was performed in 10% perchloric acid solution. The voltage of electrolysis was 18 V, and the temperature was kept at 253 K during the whole experiment [16]. The time was not limited until the light transmittance reached 200 and the instrument was stopped. TEM experiments were performed using an FEI Tecnai F20 microscope operated at 200 kV.

The dimension of samples for hardness test was 10 mm × 10 mm × 5 mm, and the surfaces were ground to 2000 mesh; and the hardness was tested by Rockwell hardness tester. Dogbone-shaped specimens with typical dimensions were machined, and tensile tests were performed on Shimadzu AGS100 at a cross-head speed of 1 mm/min. Under specific heat treatment conditions, three samples for tensile test have been tested to ensure repeatability and reliability. The sample size for the corrosion resistance test was 50 mm × 25 mm × 5 mm. A 3-mm diameter hole was drilled in the upper part of the sample for easy suspension. To eliminate the effects of surface roughness, it was sanded and then tested by dipping in a solution that mimicked sea water. Thermodynamics and kinetics calculations were performed using the software Thermo-Calc combined with the TCFE9 database. The kinetics simulations were performed using the diffusion-controlled transformations (DICTRA) simulation package

Table 1 Chemical compositions of the experimental steels (wt%)

Steel	C	N	Ni	Cr	V	Fe
C0.1N0.1	0.094	0.1075	6.45	12.2	0.219	Bal.
C0.2	0.204	0.0050	6.58	12.4	0.213	Bal.

implemented in Thermo-Calc together with the MOBFE4 database for the mobility of the elements in bcc-Fe.

3 Results and Discussion

3.1 Effect of Precipitates on the Strength and Ductility

Thermo-Calc software was used to calculate the equilibrium phase diagrams of the experimental steels, as shown in Fig. 1. Based on the phase diagrams, phase transformation in the process of solution treatment has been predicted. In C0.1N0.1 steel, V (C, N) phase with face-centered cubic structure precipitated firstly, and $Cr_{23}C_6$, Cr_2N, (Cr, V) N precipitated in sequence. A large amount of $Cr_{23}C_6$ phase precipitated in C0.2 steel. By comparing the phase diagrams of the two steels, it is not difficult to see that the VN is generated at a high quite temperature [17] (~ 1473 K) in C0.1N0.1 steel. This indicates that it is difficult to eliminate the VN generated in the solidification process via solution treatment. In C0.2 steel, the precipitation temperature is much lower (1253 K) due to the lack of nitrogen. This indicates that VC precipitates can be basically eliminated at 1273 K during the solution treatment.

Figure 2a shows the Rockwell hardness of the two steels at different heating stages. The results show that nitrogen has little effect on the Rockwell hardness of the steels at solid solution condition, but the strength and ductility are slightly different according to the tensile test results. This may be due to the fact that Rockwell hardness actually reflects the mechanical response of local areas. In addition, the size of prior austenite grains in C0.1N0.1 and C0.2 samples was quantitatively calculated, because grain size is an essential factor determining the mechanical properties of steels. The addition of nitrogen led to the presence of high-temperature

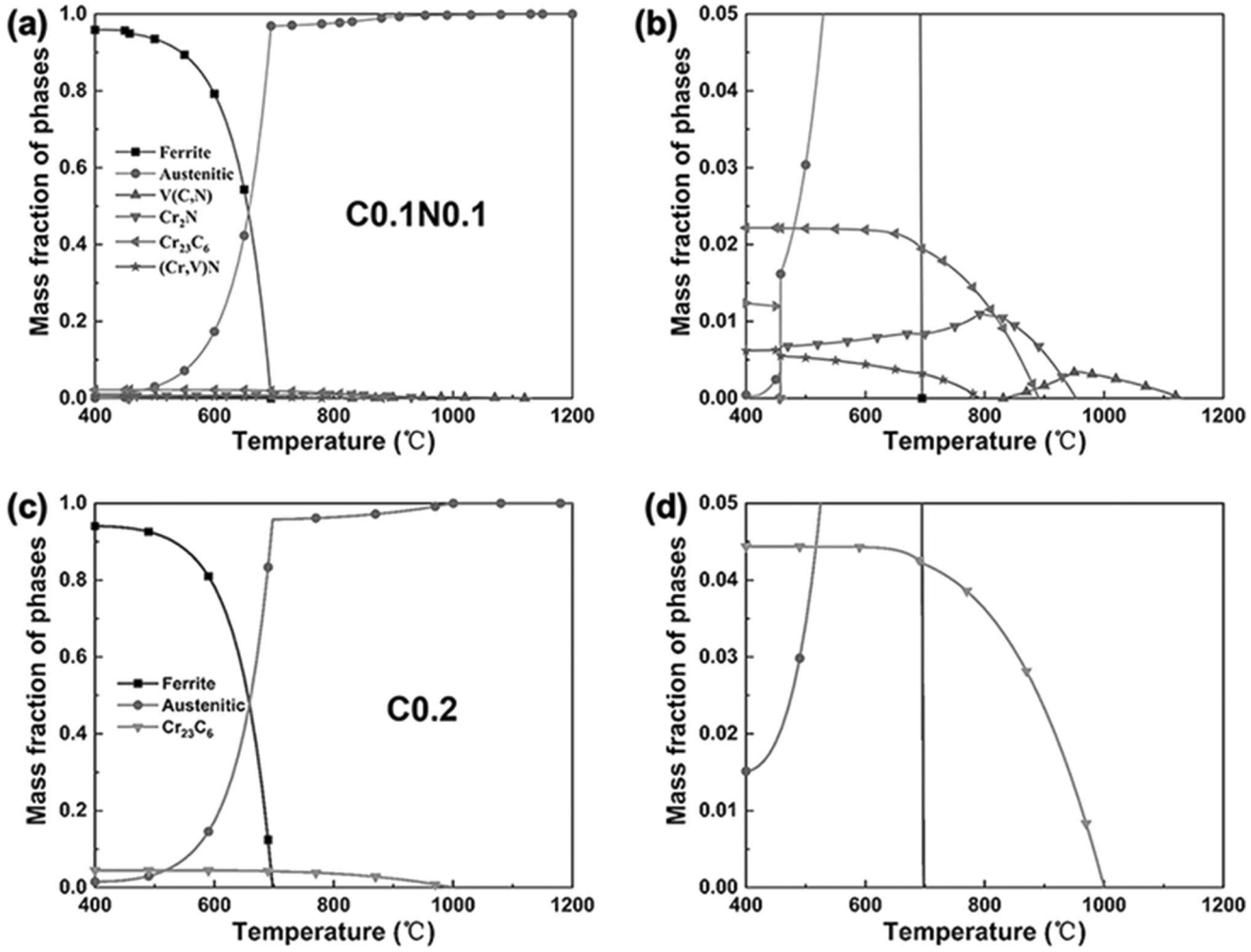

Fig. 1 Equilibrium phase fraction variations with temperature predicted by Thermal-Calc for **a** C0.1N0.1 steel and **b** detail enlarged picture of C0.1N0.1 steel; **c** C0.2steel and **d** detail enlarged picture of C0.2 steel

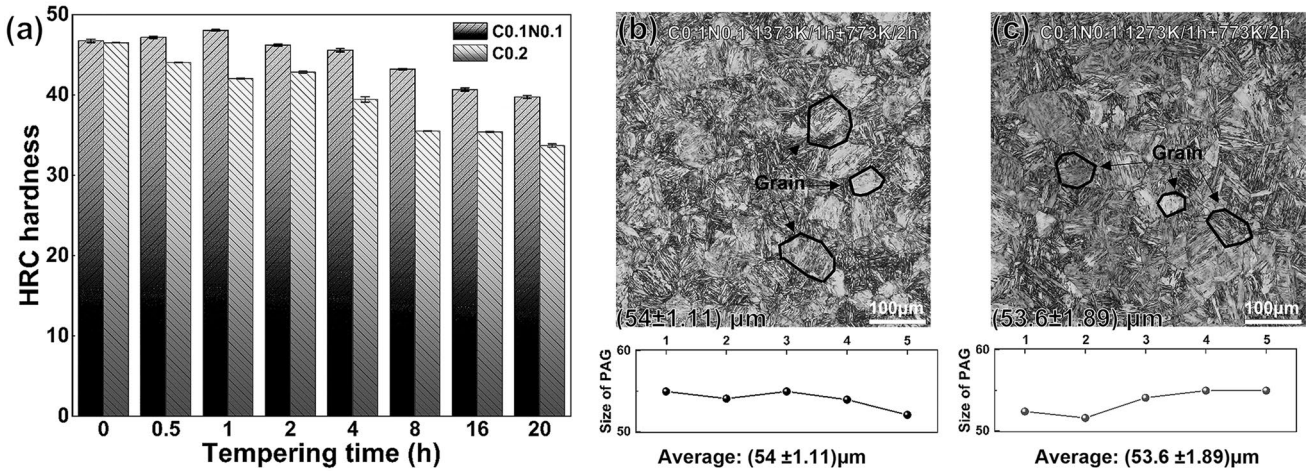

Fig. 2 **a** Evolution of hardness as a function of tempering time in two experimental steels. Error bars correspond to one standard deviation from the mean value. **b**, **c** Optical images taken for counting the size of prior austenite grain (PAG) in C0.1N0.1 and C0.2 specimens, as well as the statistical results

precipitates in the steel, which acted as nails to hinder grain growth [18, 19]. In order to more accurately evaluate the influence of the nitrogen-containing particles on the performance of the experimental steel, we changed the heat treatment route to obtain the equal grain size of the two steels, so as to eliminate the influence of grain boundary as much as possible [20–22]. According to the statistical results in Fig. 2b, c, the prior austenite grain sizes in C0.1N0.1 and C0.2 samples were determined to be (54 ± 1.11) μm and (53.6 ± 1.89) μm, respectively. This gap is within the standard deviation range, indicating that there is no difference in prior austenite grain size between C0.1N0.1 and C0.2 samples. Optical images revealed that the microstructure of two steels was similar, consisting of lath martensite with a slight amount of residual austenite and dispersive precipitates. By observing the microstructure of samples, it can be seen that precipitates in C0.1N0.1 could not be completely dissolved after solution treatment. While precipitates in C0.2 were completely dissolved after solution treatment. This is consistent with the results of Thermo-Calc analysis. After tempering, it is obvious that abundant fine precipitates dissolved out of both steels. Moreover, it can be seen that these precipitates distributed more dispersively in C0.1N0.1 steel [23], while aggregate precipitates have been found at the grain boundary in C0.2 steel.

It is evident from the hardness test results that C0.1N0.1 steel showed a pronounced secondary hardening trend during tempering, while the hardness of C0.2 steel decreased continuously during tempering. This is due to the precipitation of small dispersive (Cr, V)N phase in C0.1N0.1 steel in the tempering process, which plays a role in strengthening the steel by precipitate hardening mechanism [24, 25]. With the extension of tempering time, the second particles grow up, resulting in a continuous decrease in hardness. The hardness of C0.2 steel is always lower than that of C0.1N0.1 steel and the hardness of C0.2 steel is severely reduced as the tempering time is extended.

Based on the thermodynamic results, the solution treatment for C0.1N0.1 steel was chosen to be 1373 K/1 h followed by air cooling. The solution treatment of C0.2 steel has been selected as 1273 K/1 h, followed by air cooling. In this way, the grain sizes of the two steels are essentially the same, thus minimizing the effect of grain boundary. Finally, the samples used for microstructure characterization and property testing were tempered at 773 K for 2 h.

Table 2 indicates the mechanical properties of two experimental steels obtained by tensile test. The yield strength (YS), ultimate tensile strength (UTS) and elongation (EL) of C0.1N0.1 sample are (866 ± 7) MPa, (1604 ± 9) MPa and (15 ± 1)%, respectively. Meanwhile, the YS, UTS and EL of C0.2 sample are (859 ± 5) MPa, (1416 ± 8) MPa and (12.8 ± 0.2)%, respectively. It turns out that the properties of two steels differ considerably after tempering. The ultimate tensile strength of C0.1N0.1 sample decreases slightly, but the elongation increases significantly, which may be attributed to the occurrence of dispersive precipitates during tempering [26, 27]. It is noteworthy that substituting 0.1% carbon by 0.1% nitrogen contributes to the simultaneous enhancement of UTS (190 MPa) and EL (2.2%) compared with C0.2 sample. While

Table 2 Mechanical property of the experimental steels

Steel	YS (MPa)	UTS (MPa)	EL (%)	AR (%)
C0.1N0.1	866 ± 7	1604 ± 9	15 ± 1	63.7 ± 1
C0.2	859 ± 5	1416 ± 8	12.8 ± 0.2	62.5 ± 1

YS and area reduction (AR) are basically the same. In addition, it can be seen from the fracture morphology in Fig. 3b and c that the fracture character of C0.1N0.1 and C0.2 samples is a mixture of dimple and cleavage plane. The difference is that C0.1N0.1 sample has a much higher percentage of cleavage features, which seems slightly different from the better strength/ductility combination of C0.1N0.1 sample shown in Table 2. In this regard, it is believed that carbonitrides should be the main factor controlling strength and ductility. Work hardening often occurs when engineering strain increases during tensile test and the microstructure mechanism should be attributed to the dislocation multiplication and plug, which is prone to cleavage fracture mode. Attributed to the nitrogen alloying, dispersive carbonitrides in C0.1N0.1 steel make the stress distribution in the deformation process more uniform and delays the necking and fracture caused by stress concentration [28]. Therefore, although C0.1N0.1 shows a higher proportion of cleavage fracture characters, it still behaves better ductility than that of C0.2 steel [29, 30]. Considering the fracture of C0.2 sample, ductile fracture with the micro-void aggregation mode accounts for a large proportion. However, the existence of large-size precipitates was prone to cause stress concentration and facilitate the generation and propagation of microcracks in steel, which led to the reduction of strength and elongation of C0.2 sample.

Figure 4a–d is SEM images indicating carbonitrides in C0.1N0.1 and C0.2 samples. It can be clearly seen that there are significant differences in the precipitates characters between C0.1N0.1 and C0.2 samples. The amount of precipitates in C0.1N0.1 sample is much less than that in C0.2 sample. Based on this phenomenon, it is concluded that the partial substitution of carbon by nitrogen is effective in suppressing the precipitation of carbonitride. In addition, it can be observed that accumulation precipitates have been observed at the grain boundary in C0.2 sample. In comparison, the grain boundary of C0.1N0.1 sample is clean and rare precipitates could be observed along the grain boundary. The results indicate that nitrogen can inhibit the precipitation at prior austenite grain boundary (PAGB) and promote the precipitation in the inner grain area, thus making the distribution of carbonitride in high nitrogen martensitic steel more dispersed. A conclusion can be drawn that the strength and plasticity of steel can be improved simultaneously by the fine and dispersed precipitated phase.

3.2 Effect of Nitrogen Alloying on the Ability of Martensitic Stainless Steel Against Pitting Corrosion

According to the experimental results, the corrosion rate of C0.1N0.1 is 0.1324 g/(h m^2) and that of C0.2 is 0.4153 g/(h m^2). The results show that the corrosion resistance of C0.1N0.1 steel is better.

Figure 5a and c shows the macroscopic morphology of samples after immersion test. The surface of C0.1N0.1 sample showed few corrosion traces and remained bright as a whole, while the surface of C0.2 sample showed large corrosion traces and a large amount of corrosion products accumulated around the corrosion pit. The maximum pitting was observed by metallography, and the results are shown in Fig. 5b and d. The pitting pit depth of C0.2 sample was 110 μm, while that of C0.1N0.1 sample was only 50 μm. By comparison, it could be seen that the surface of C0.2 sample was more seriously corroded than that of C0.1N0.1 sample. It can be seen that adding nitrogen into steel can effectively improve its corrosion resistance. The higher resistance to pitting corrosion of tempered C0.1N0.1 steel is apparently due to the lower content of harmful large-size precipitates. The dispersive fine precipitates and the reduced aggregation at grain boundaries contribute to the lower acidity and weaker aggressiveness of the test solution near the sample surface due to the accumulation of NH^{4+} ammonium ions in it [31].

The better pitting resistance of C0.1N0.1 steel should be attributed to the intrinsically beneficial effect of nitrogen which has been widely reported in previous research. What is more, the precipitates should be the main factor leading to the different corrosion resistance of two martensitic stainless

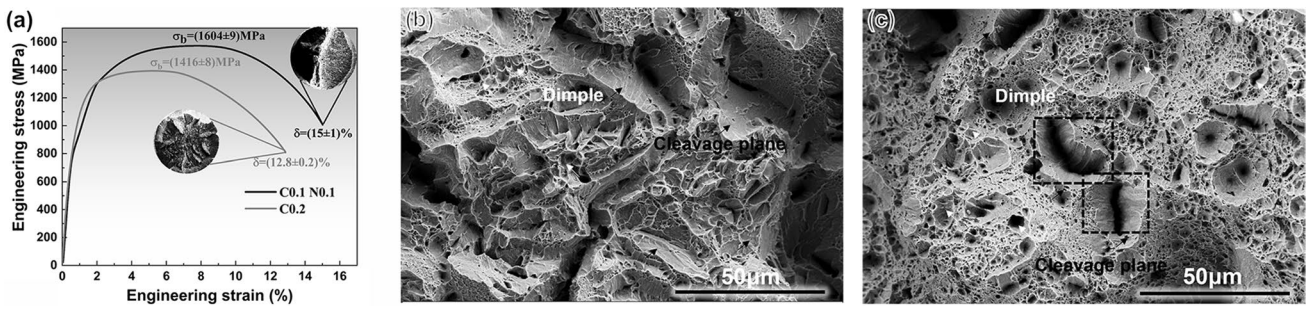

Fig. 3 **a** Engineering stress–strain curves of C0.1N0.1/C0.2 specimens after tempering treatments; **b**, **c** corresponding fracture morphologies observed by SEM

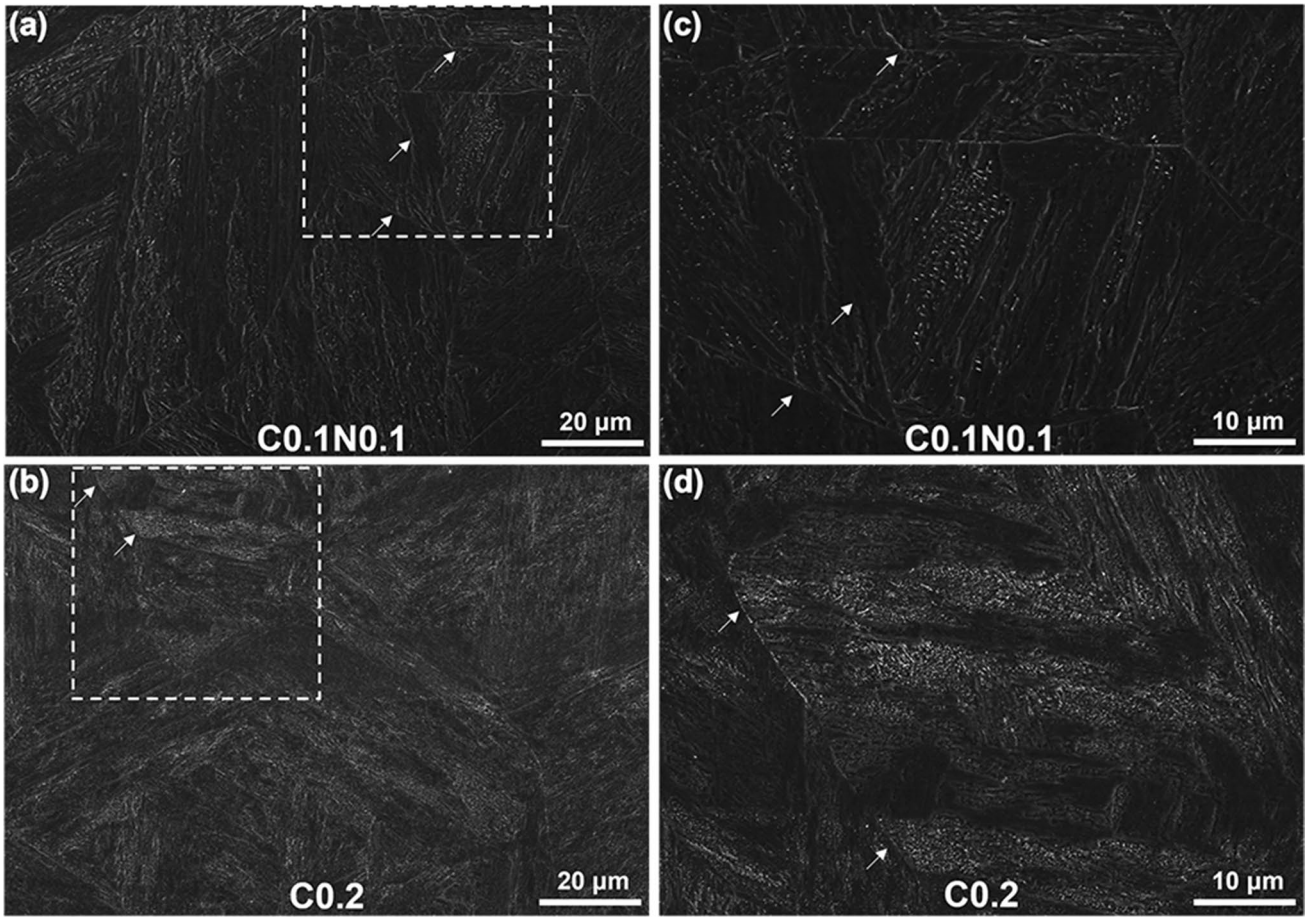

Fig. 4 SEM images indicating carbonitrides in C0.1N0.1 specimen **a** and **c**, and carbonitrides in C0.2 specimen **b**, **d**

steels. In C0.2 steel, the precipitates after tempering are mainly $Cr_{23}C_6$ and it can be seen from Fig. 6a, b that the amount of precipitates in C0.2 sample is much more than that in C0.1N0.1 sample, which will cause the generation of serious chromium depletion area [31, 33]. There is no doubt that Cr is the main element in improving the corrosion resistance of steel, while its content in matrix will be severely reduced once the Cr atoms dissolve out to form precipitates. When nitrogen is added into carbon steel, the types of precipitates change into Cr_2N [34], V(N,C) and $Cr_{23}C_6$, demonstrated by thermodynamic calculations. Furthermore, the addition of nitrogen can inhibit the precipitation of carbides, thus slowing down the decreasing trend of chromium content in matrix [35, 36] and improving the corrosion resistance of C0.1N0.1 steel after tempering treatment.

In order to further understand the relationship between characters of precipitates and the corrosion resistance, the differences in the number and type of precipitates between C0.1N0.1 and C0.2 samples were subtly compared by TEM characterizations. Typical bright field images of C0.1N0.1 sample clearly show dense carbonitrides, as shown in Fig. 7a. At higher magnification, scanning transmission electron microscopy (STEM) and energy dispersive spectroscopy (EDS) mapped by Cr, N, C and V atoms outline the morphology of the carbonitrides. The carbide distribution features were observed in C0.2 sample. The morphology of carbide can be observed in Fig. 8a, c. It can be seen that the size of precipitates in C0.2 steel is slightly larger than that of C0.1N0.1 sample, which is consistent with the previous SEM observations. It should also be noted that the precipitate in C0.1N0.1 steel mainly consists of Cr, N, C and V, while the precipitate in C0.2 sample mainly consists of Cr and C.

The partial replacement of carbon with nitrogen contributed to an increase in ductility and strength of the steel, apparently due to the formation of more dispersive carbonitrides during tempering, as well as a slight increase in residual austenite in the form of thin layers between the martensite lath. These film-like austenites should have not undergone $\gamma \rightarrow \alpha$ transformation [37, 38] due to random increased compressive stresses.

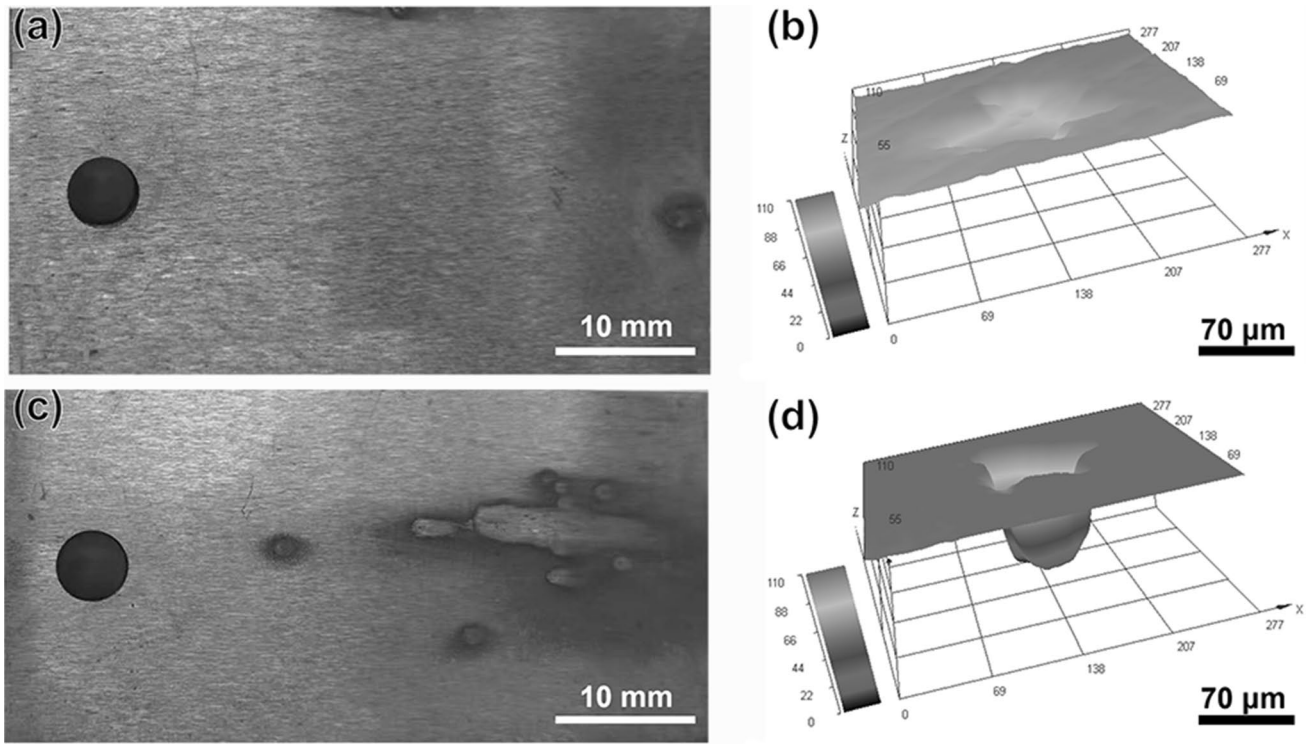

Fig. 5 **a** and **c** Macroscopic morphologies after immersion in 3.5% NaCl solution at 303 K. **b**, **d** Depth of maximum pitting pit of C0.1N0.1 and C0.2

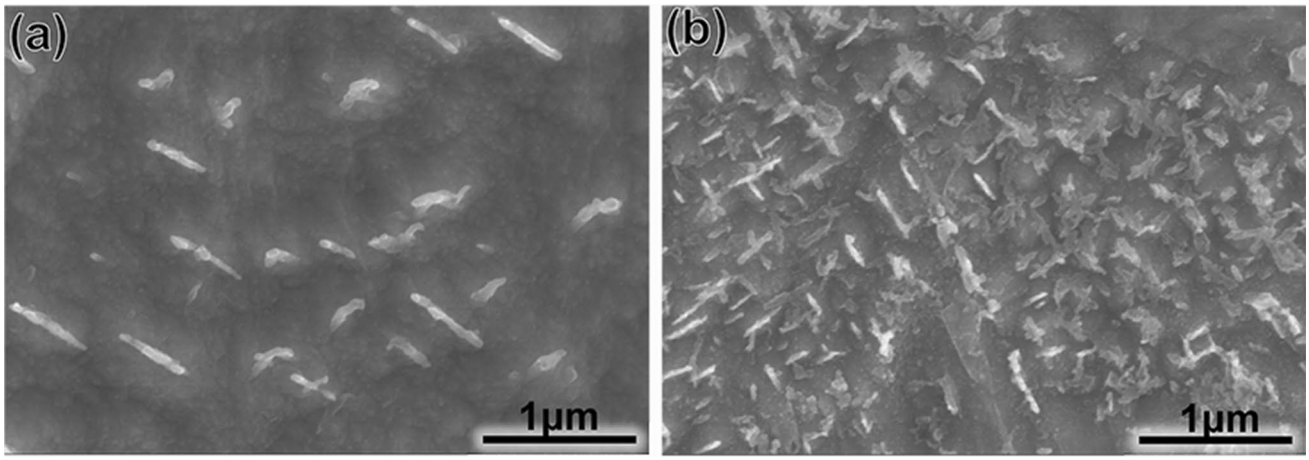

Fig. 6 SEM images of **a** C0.1N0.1, **b** C0.2 samples after tempering treatment

3.3 Understanding the Effect of Nitrogen on the Precipitates Based on Thermodynamic and Kinetic Simulations

Table 3 lists the percentage content of the different phases after tempering at 773 K. The results show that $Cr_{23}C_6$ and Cr_2N are the main Cr-rich precipitates in the experimental steels, which is consistent with the previous microstructure characterizations. In addition, the content of $Cr_{23}C_6$ type carbides decreases obviously when partially substitute carbon by nitrogen. Furthermore, the addition of nitrogen enriches the type of precipitate in the steel. Since different precipitates are not easy to aggregate and grow up because of the composition difference, the size of precipitates in C0.1N0.1 sample is smaller than that in C0.2 sample [39]. Moreover, the variety of precipitates is more likely to generate

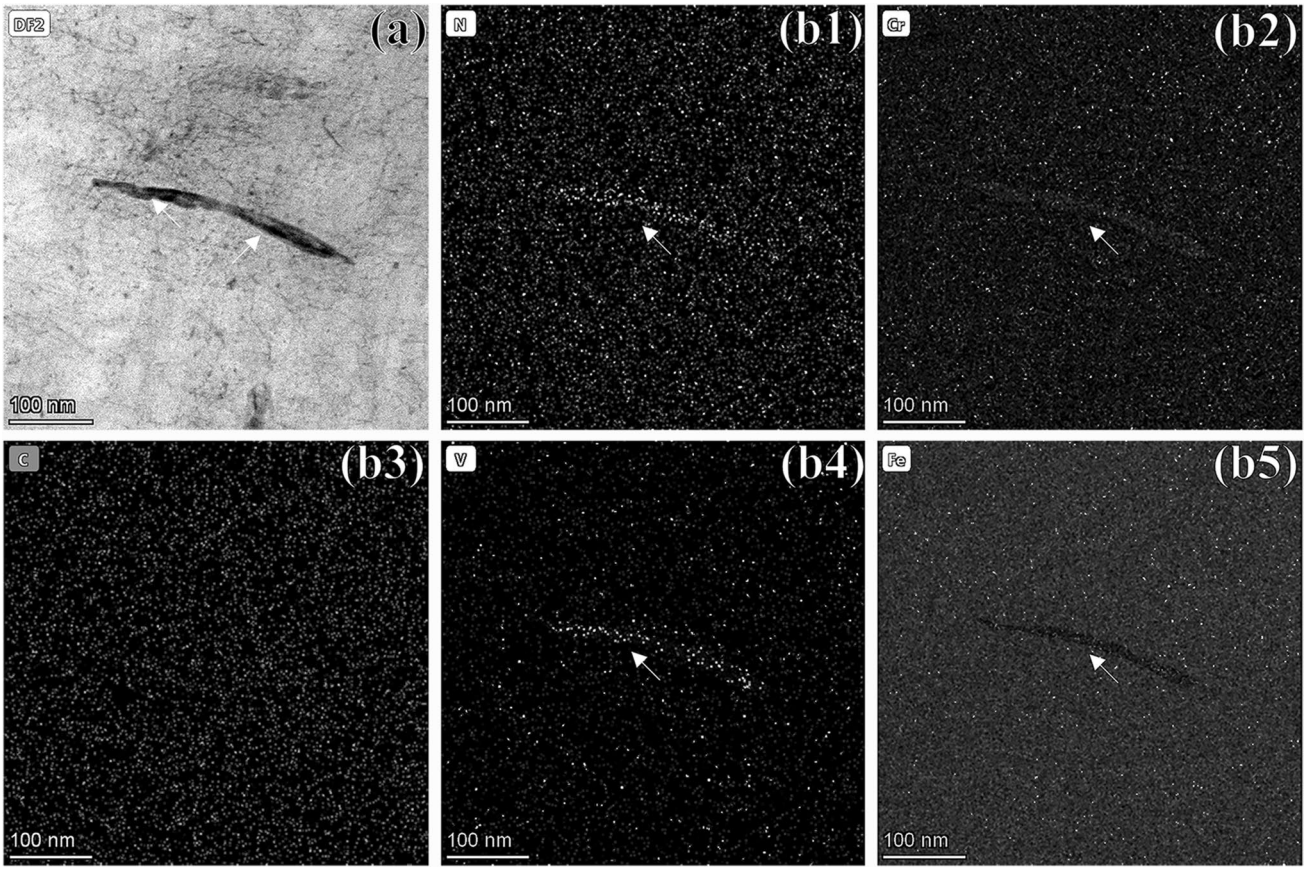

Fig. 7 TEM images taken from C0.1N0.1 sample after tempering treatment showing N, Cr, C, V and Fe element mappings

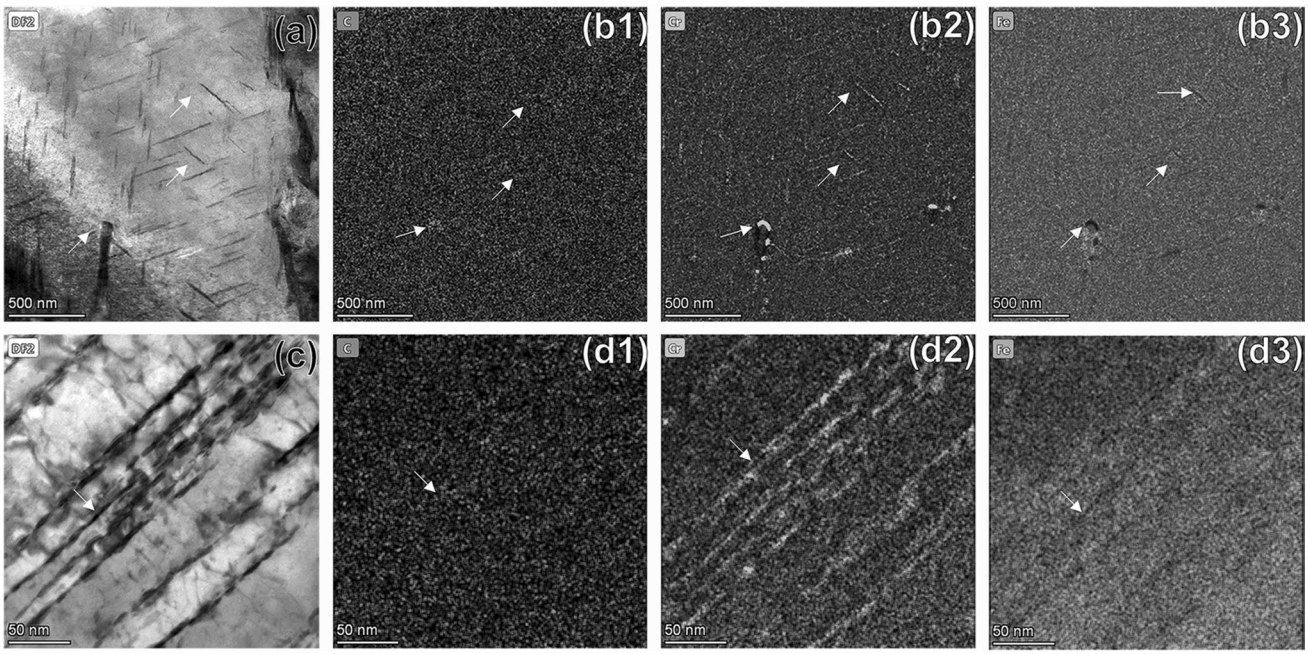

Fig. 8 TEM micrographs for C0.2 and the corresponding STEM EDS of C, Cr and Fe element mappings

Table 3 Percentage of various phases at 773 K (%)

Steel	Ferrite	Austenite	$Cr_{23}C_6$	Cr_2N	(Cr,V)N
C0.1N0.1	94.898	2.4692	1.7629	0.42324	0.44659
C0.2	93.505	2.9496	3.5457	0	0

dispersive distribution character, which leads to a stronger precipitation hardening effect in C0.1N0.1 sample than that in C0.2 sample.

The SEM results show that substituting carbon by nitrogen in martensitic stainless steel could promote the intragranular precipitates during tempering. At the same time, attributed to the nitrogen alloying effect, the precipitates at grain boundary will be suppressed and the dispersive precipitates could be obtained. According to TEM results in C0.1N0.1 steel, the types of precipitates changed after tempering treatment. The change of precipitate type caused by the addition of nitrogen should be key factor causing more dispersive precipitates in C0.1N0.1 steel [40], thus leading to superior combination of strength, ductility and corrosion resistance. In order to deepen the functional mechanism of nitrogen on the precipitates in the steel, we carried out relevant thermodynamic calculations. Figure 9 shows the variation of Gibbs free energy of each precipitate in the sample with nitrogen content. According to thermodynamic calculation results, we can see clearly that when C/N ratio is lower, the Gibbs free energy of nitride is reduced gradually, and carbide Gibbs free energy gradually increases. This could well explain the effective increase in precipitate type by substituting carbon by nitrogen, as well as the suppression of precipitation and aggregation of $Cr_{23}C_6$ precipitates in martensitic stainless steel.

In addition, the variation of Gibbs free energy of $Cr_{23}C_6$ with nitrogen content was calculated when carbon content was fixed at 0.1%, shown in Fig. 9b. It was found that nitrogen inhibited the precipitation of $Cr_{23}C_6$ and this indicated that nitrogen addition could reduce the number of coarse carbides $Cr_{23}C_6$ in C0.1N0.1 steel. According to thermodynamic calculation results, substituting carbon by nitrogen in martensitic stainless steel, the driving force of $Cr_{23}C_6$ precipitates would weaken dramatically; meanwhile, the driving force of (Cr, V) N and Cr_2N could be enhanced. Therefore, under the same tempering conditions, both the size and quantity of precipitates in C0.1N0.1 steel are smaller than that in C0.2 steel.

Nitrogen was found to suppress the precipitation of carbide at the grain boundaries in C0.1N0.1 steel. In view of this phenomenon, the diffusion coefficient of carbon in BCC-Fe under different ratios of carbon and nitrogen and the diffusion coefficient of carbon in BCC-Fe with various nitrogen content when carbon content was fixed at 0.1% were calculated, shown in Fig. 10. It was found that the addition of nitrogen element inhibited the diffusion of carbon in BCC-Fe, which indicated that it will be more difficult for carbon atoms to diffuse toward grain boundaries. That is, the probability of forming carbides at the grain boundaries decreased. Therefore, nitrogen alloying improves the distribution of carbide along grain boundaries.

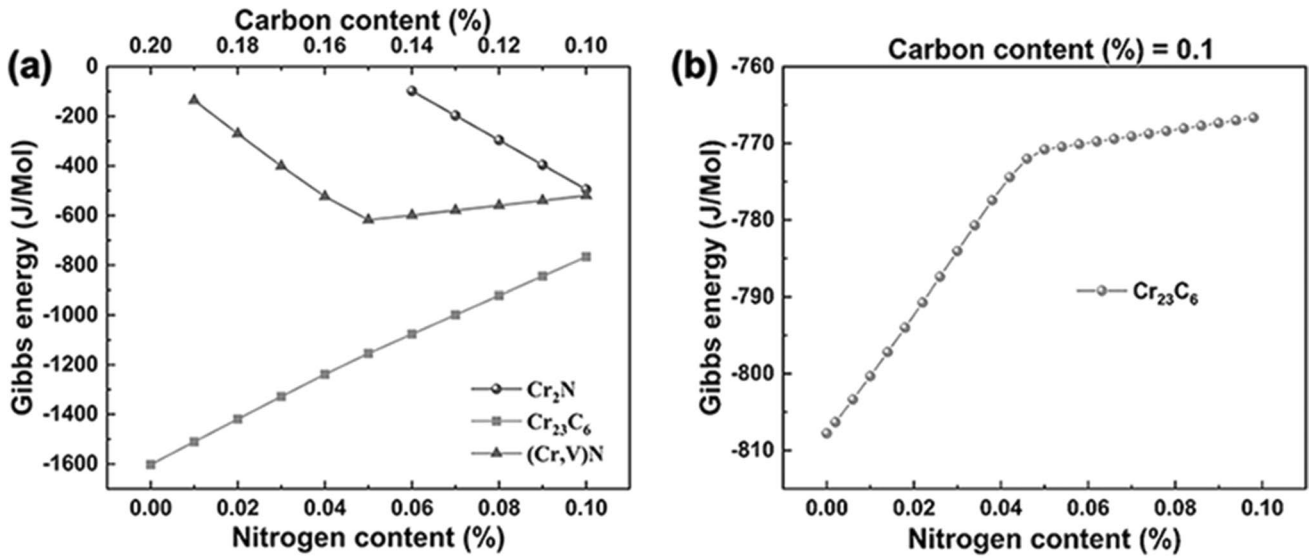

Fig. 9 Thermal-Calc simulation on Gibbs free energy of the precipitated phase with the (C + N) = 0.2 composition at 500 °C as a function of the nitrogen content. **a** Gibbs free energy of (Cr,V)N, Cr_2N and $Cr_{23}C_6$, **b** Gibbs free energy of $Cr_{23}C_6$ with nitrogen content when carbon is fixed

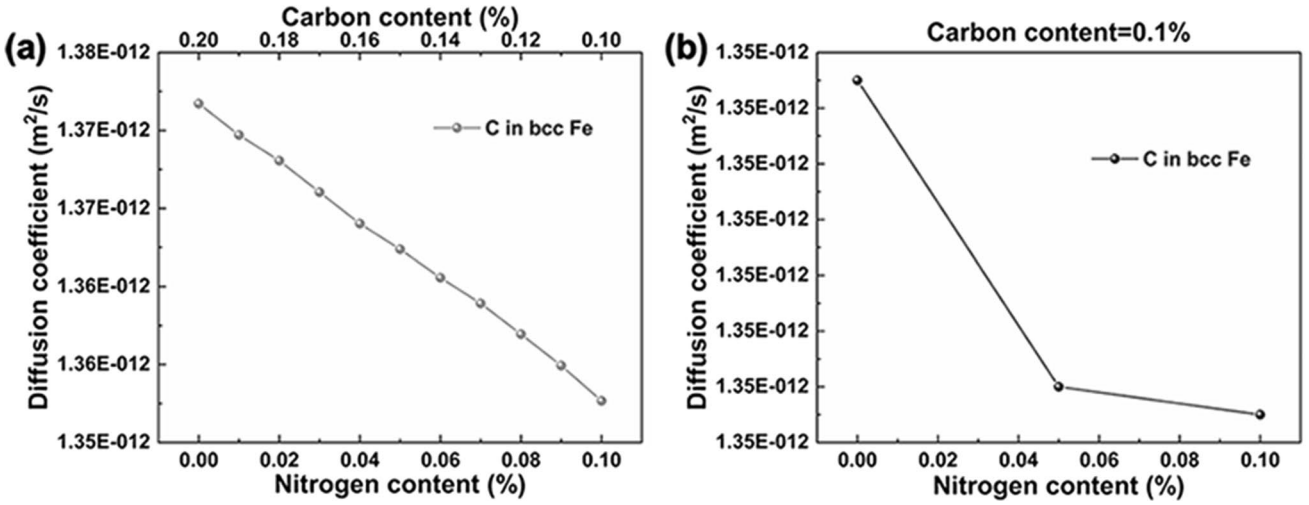

Fig. 10 Thermal-Calc simulation on diffusion coefficient of **a** the BCC with the (C + N) = 0.2 composition as a function of the nitrogen content at 773 K, **b** the BCC as a function of the nitrogen content at 773 K when carbon is fixed

3.4 Microstructure Evolution in the Tempering Process

Based on the above experimental results and thermodynamic calculations, the microstructure evolution of the experimental steels during the heat treatment is illustrated in Fig. 11. Subjected to solution treatment, fully austenite microstructure with no precipitates could be obtained, shown in Fig. 11a. In the subsequent air-cooling process, martensitic transformation begins when the temperature is lowered to the martensitic transformation start temperature (*M*s), as shown in Fig. 11b1, c1. When air cooling to room temperature, typical lath martensite microstructure containing a small amount of retained austenite has been obtained (Fig. 11b2, c2) in both C0.1N0.1 and C0.2 steels.

In the tempering process, solute atoms (Cr and C) in C0.2 steel will precipitate from the matrix (Fig. 11e2); meanwhile, Cr and C atoms will diffuse toward the grain boundary to form carbides (Fig. 11e3). In comparison, substituting carbon by nitrogen (C0.1N0.1 steel) increases the Gibbs energy of $Cr_{23}C_6$ carbides and inhibits their precipitation in the tempering process. In addition, the change of C/N ratio reduces

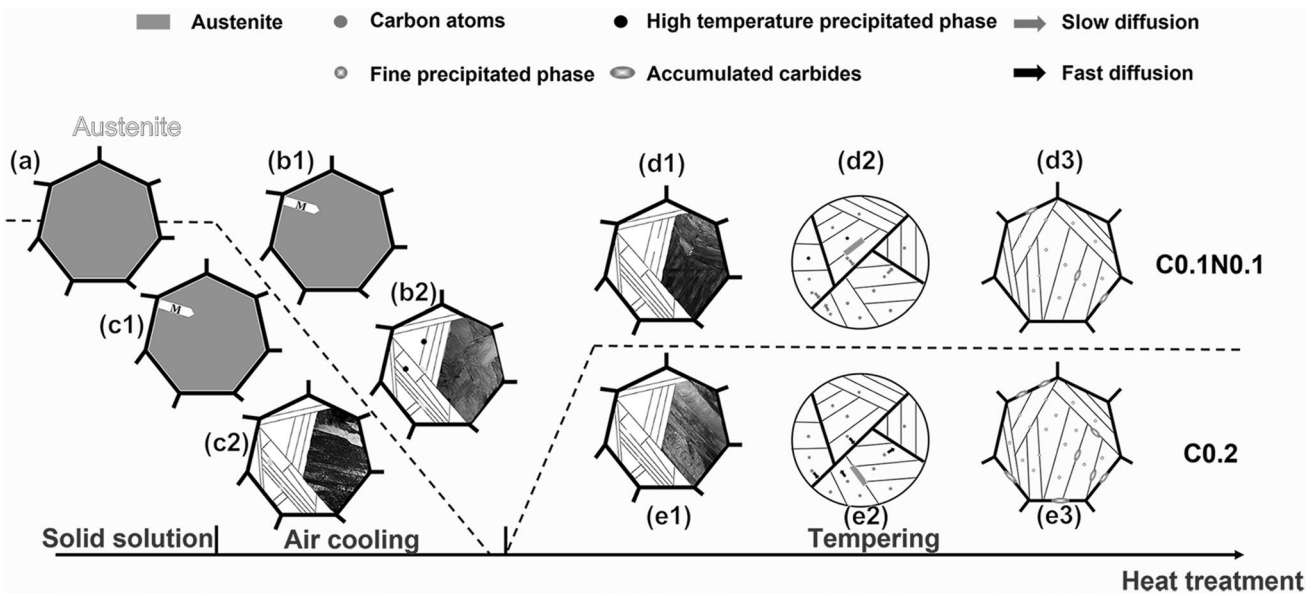

Fig. 11 Microstructure evolution of experimental steels during the heat treatment

the diffusion rate of C, which has a significant effect on the redistribution of C atoms during tempering (Fig. 11d2), which can effectively reduce the aggregation of carbonitride at grain boundaries (Fig. 11d3). As a result, more dispersive carbonitrides have been obtained in C0.1N0.1 steel.

4 Conclusions

1. Systematic experimental studies associating with thermodynamic and kinetic simulations demonstrated that the optimization of the chemical composition of 2Cr12Ni6 (C0.2) martensitic stainless steel via partial replacement 0.1% carbon by 0.1% nitrogen (C0.1N0.1 steel) contributed to increasing its strength, ductility and corrosion resistance. After composition optimization, an increase of UTS (190 MPa) and EL (2.2%) has been achieved in C0.1N0.1 steel. The increase in pitting resistance in a 3.5% NaCl solution at 303 K (modeling sea water solution) was characterized by a significant reduction in the number of pittings on the surface of the C0.1N0.1 sample and a reduction of more than twofold (from 110 to 50 microns) considering the depth of pittings.
2. Improvement of mechanical properties in C0.1N0.1 steel should be attributed to the changes in the type, size, quantity and distribution of carbides and carbonitrides formed during tempering. Uniform distribution of carbonitrides in C0.1N0.1 steel with weak grain boundary aggregation has contributed to this improvement.
3. Improvement of pitting resistance of C0.1N0.1 steel is caused by reducing the aggregation of high-chromium carbides. This will suppress the occurrence of chromium depletion area and motivate the inhibitory effect of NH_4^+ ammonium ions formed during dissolution of steel.
4. Regulation of carbon and nitrogen in the martensitic stainless steels can effectively tailor the free Gibbs energy of various phases and diffusion rates of precipitate-forming elements, promoting the formation of more dispersive carbonitrides and weakening their aggregation at the grain boundary.

Acknowledgements This work was supported by the Fundamental Research Funds for the National Natural Science Foundation of China (No. 52004059), the Program of Introducing Talents of Discipline to Universities (No. B21001), the Central Universities (No. N2125017), and the Talent Project of Revitalizing Liaoning (No. XLYC1902046). We acknowledge Dr. Lifeng Zhang for TEM characterizations support and the discussion on evolution of carbonitrides.

Declarations

Conflict of interest The authors state that there are no conflicts of interest to disclose.

References

[1] J. Guo, C.J. Shang, S.W. Yang, Y. Wang, L.W. Wang, X.L. He, J. Iron Steel Res. Int. **63**, 16 (2009)
[2] Y.T. Xi, D.X. Liu, D. Han, Acta Metall. Sin. -Engl. Lett. **21**, 21 (2008)
[3] H. Zheng, X.N. Ye, J.D. Li, L.Z. Jiang, Z.Y. Liu, G.D. Wang, B.S. Wang, Mater. Sci. Eng. A **7407**, 527 (2010)
[4] A. Akhiate, E. Braud, D. Thibault, Carbon content and heat treatment effects on microstructures and mechanical properties of 13%Cr–4%Ni martensitic stainless steel. Conf. Metall. (2014).
[5] S.H. Li, K.Y. Zhao, K. Wang, M.S. Yang, Mater. Charact. **154**, 124 (2017)
[6] J.B. Wang, Y.F. Zhou, X.L. Xing, S. Liu, C.C. Zhao, Y.L. Yang, Q.X. Yang, Surf. Coat. Technol. **115**, 294 (2016)
[7] H. Feng, H.B. Li, W.C. Jiao, Z.H. Jiang, M.H. Cai, H.C. Zhu, Z.G. Chen, Metall. Mater. Trans. A **4987**, 50 (2019)
[8] R.C. Fan, M. Gao, Y.C. Ma, X.D. Zha, X.C. Hao, K. Liu, J. Mater. Sci. Technol. **1059**, 28 (2012)
[9] F. Shi, L.J. Wang, W.F. Cui, C.M. Li, Acta Metall. Sin. -Engl. Lett. **95**, 20 (2007)
[10] X.P. Ma, L.J. Wang, B. Qin, C.M. Liu, S.V. Subramanian, Mater. Eng. (Reigate U. K.) **74**, 34 (2011)
[11] Y.T. Chen, A.M. Guo, L.X. Wu, J. Zeng, P.H. Li, Acta Metall. Sin. -Engl. Lett. **57**, 19 (2006)
[12] H. Berns, R. Ehrhardt, Steel Res. Int. **343**, 67 (1996)
[13] V.G. Gavriljuk, Mater. Sci. Eng. A **75**, 438 (2006)
[14] W.C. Jiao, H.B. Li, J. Dai, H. Feng, Z.H. Jiang, T. Zhang, D.K. Xu, H.C. Zhu, S.C. Zhang, J. Mater. Sci. Technol. **2357**, 35 (2019)
[15] Z.H. Jiang, H. Feng, H.B. Li, H.C Zhu, S.C. Zhang, B.B. Zhang, Y. Han, T. Zhang, D.K. Xu, Materials **861**, 10 (2017)
[16] J.L. Tian, K. Chen, H.B. Li, Z.H. Jiang, Mater. Sci. Eng. A **142529**, 833 (2021)
[17] H.C. Wang, Y.J. Li, E. Detemple, G. Eggeler, Scr. Mater. **350**, 187 (2020)
[18] H.B. Wu, H.T. Jiang, S.W. Yang, D. Tang, X.L. He, Acta Metall. Sin. -Engl. Lett. **313**, 20 (2007)
[19] D.W. Tian, L.P. Karjalainen, B. Qian, Metall. Mater. Trans. A **4031**, 27 (1996)
[20] J.W. Morris Jr, The influence of grain size on the mechanical properties of steel. In *Proceedings of the International Symposium on Ultrafine Grained Steels*, e. by S. Takaki, T. Maki (Iron and Steel Institute, Tokyo 2001), p. 34
[21] L.W. Tsay, H.L. Lu, C. Chen, Corros. Sci. **2506**, 50 (2008)
[22] J. Gu, L.X. Zhang, S. Ni, Micron **93**, 105 (2018)
[23] S.C. Krishna, N.K. Karthick, A.K. Jha, B. Pant, P.V. Venkitakrishnan, Metall. Microstruct. Anal. **425**, 6 (2017)
[24] H.M. Geng, X.C. Wu, Y.A. Min, H.B. Wang, H.K. Zhang, Acta Metall. Sin. -Engl. Lett. **43**, 21 (2008)
[25] A. Toro, W.Z. Misiolek, A.P. Tschiptschin, Acta Mater. **3363**, 51 (2003)
[26] B.B. Zhang, F.K. Yan, M.J. Zhao, N.R. Tao, K. Lu, Acta Mater. **310**, 151 (2018)
[27] X.P. Ma, L.J. Wang, C.M. Liu, S.V. Subramanian, Mater. Sci. Eng. A **271**, 539 (2012)
[28] J.S. Wang, M.D. Mulholland, G.B. Olson, D.N. Seidman, Acta Mater. **4939**, 61 (2013)
[29] Z.M. Wang, H. Li, Q. Shen, W.Q. Liu, Z.Y. Wang, Acta Mater. **158**, 156 (2018)
[30] A. Lass Eric, F. Zhang, E. Campbell Carelyn, Metall. Mater. Trans. A **2318**, 51 (2020)
[31] H. Feng, Z.H. Jiang, H.B. Li, P.C. Lu, S.C. Zhang, H.C. Zhu, B.B. Zhang, T. Zhang, D.K. Xu, Z.G. Chen, Corros. Sci. **288**, 144 (2018)

[32] Y.G. Zhao, W. Liu, T.Y. Zhang, Z.T. Sun, Y.B. Wang, Y.M. Fan, B.J. Dong, Corros. Sci. **109580**, 189 (2021)
[33] X. He, X.Y. Lu, Z.W. Wu, S.H. Li, Q.L. Yong, J.X. Liang, J. Su, L.X. Zhou, J. Li, K.Y. Zhao, J. Iron Steel Res. Int. **629**, 28 (2021)
[34] T.Y. Sun, Y.J. Guo, Y.M. Jiang, J. Li, Acta Metall. Sin. -Engl. Lett. **755**, 32 (2019)
[35] M.B. Khashayar, Z. Nika, N. Pooria, P. Mahmoud, Corros. Sci. **109340**, 183 (2021)
[36] V.G. Gavriljuk, B.D. Shanina, H. Berns, Mater. Sci. Eng. A **707**, 481 (2006)
[37] S.G. Wang, X. Wang, L.X. Hua, Z.W. Liu, H.L. Zhou, J. Univ. Sci. Technol. B **7**, 2 (1995)
[38] V.I. Levitas, D.L. Preston, Phys. Rev. B **134206**, 66 (2002)
[39] W.B. Tian, D. Wu, Y.Y. Li, S.P. Lu, Acta Metall. Sin. -Engl. Lett. **577**, 35 (2022)
[40] J.G. Chen, Y.C. Liu, Y.T. Xiao, Y.H. Liu, C.X. Liu, H.J. Li, Acta Metall. Sin. -Engl. Lett. **706**, 31 (2018)